Applied Catalysis B: Environmental 187 (2016) 204–211

Contents lists available at ScienceDirect

Applied Catalysis B: Environmental

journal homepage: www.elsevier.com/locate/apcatb

Photocatalytic performance of $BiPO_4$ nanorods adjusted via defects

Yanyan Zhu[a,b], Qiang Ling[b], Yanfang Liu[c], Hua Wang[b], Yongfa Zhu[a,*]

[a] Department of Chemistry, Beijing Key Laboratory for Analytical Methods and Instrumentation, Tsinghua University, Beijing 100084, PR China
[b] Institute of Aeronautical Meteorology and Chemical Defence, Beijing 100085, PR China
[c] Sinopec Research Institute of Petroleum Processing, Beijing 100083, PR China

ARTICLE INFO

Article history:
Received 2 November 2015
Received in revised form 4 January 2016
Accepted 9 January 2016
Available online 13 January 2016

Keywords:
Defect
$BiPO_4$
Ball-milling
Photocatalytic degradation

ABSTRACT

The effect of defect on the photocatalytic and photoelectric performance of $BiPO_4$ has been revealed. The bulk defects of $BiPO_4$ such as bismuth vacancies (V_{Bi}), oxygen vacancies (V_O) and so on were formed during the ball-milling process. These bulk defects of $BiPO_4$ inhibited the separation of photo-generated charges greatly and thus reduced photocatalytic activity. Most of the bulk defects were repaired and the photocatalytic activity of $BiPO_4$ was also recovered mostly via calcination and reflux. Reflux could repair the bulk defects of $BiPO_4$ much better than calcination. The mechanism of the photocatalytic degradation of pollutants over $BiPO_4$ was not changed by defects, and the main oxidation active species of $BiPO_4$ is photo-generated hole.

1. Introduction

As an oxy-acid salt photocatalyst, $BiPO_4$ possesses many advantages such as high photocatalytic activity, stable chemical structure, exceptional optical and electronic properties, fast rate of settlement separation and strong mineralization ability [1,2]. There are three kinds of crystal structure of $BiPO_4$ (HBIP, mMBIP and nMBIP). Among them, the photocatalytic activity of HBIP is the worst, with its band gap being 4.6 eV. mMBIP and nMBIP possess higher photocatalytic activity, and their band gaps are 4.2 eV and 3.8 eV respectively. Moreover, the photocatalytic activity of nMBIP $BiPO_4$ is much better than that of Degussa P25 TiO_2 [3,4]. To expand the absorption range and improve the photocatalytic activity of $BiPO_4$, many different kinds of methods such as doping [5], compositing [6–8], surface defects [2,9,10] and high-energy facet adjusting [11] have been employed, and they are proved to be efficient in enhancing its ultraviolet photocatalytic performance or expanding the range of absorption spectrum to visible light region.

The photocatalytic performances of semiconductor materials are mainly decided by particle size, crystal structure, band gap, lattice plane, surface area, morphology, defect and so on. Among them, defect has significant influence on the formation, separation and migration of photo-generated electrons and holes, as well as light-absorption range. There are two kinds of defects, surface defects and bulk defects [12–14]. Surface defects are shallow defects, which could quickly capture and then release photo-generated charges, and the temporary capture might accelerate the separation of photo-generated electrons and holes. In addition, surface defects are the adsorption site of O_2, which reacts with surface photo-generated electrons to form $^{\bullet}O_2^-$, and $^{\bullet}O_2^-$ will degrade organic pollutants. Therefore, surface defects not only accelerate the separation of photo-generated charges but also increase the number of active sites, and further enhancing photocatalytic activity. TiO_2 [15–20], ZnO [21,22], $BiPO_4$ [2,9,10], $Bi_6S_2O_{15}$ [23], CeO_2 [24], $Zn_xCd_{1-x}S$ [25] and Bi_2MO_6 [26] with surface defect synthesized via vacuum de-oxygen, high temperature calcination and hydrogen reduction possess not only superior UV photocatalytic performance but also wide light absorption range. As deep defects, bulk defects capture photo-generated charges but do not release them easily, which become the recombination center of photo-generated charges and further decrease the photocatalytic performance [13,14,27]. Defects widely exist in the semiconductor photocatalyst materials as an inherent structure. Therefore, it is of great value to study the effect of defect on the photocatalytic performance of semiconductor materials.

In this work, the defects in $BiPO_4$ were controllably formed via adjusting ball-milling time and rate, and most of them could be repaired via calcination and reflux in water. The influence of defects on the photocatalytic and photoelectric performances of $BiPO_4$ was revealed. The mechanism for the effect of defects on the photocatalytic activity of $BiPO_4$ was also investigated.

* Corresponding author.
E-mail address: zhuyf@mail.tsinghua.edu.cn (Y. Zhu).

http://dx.doi.org/10.1016/j.apcatb.2016.01.012
0926-3373/

2. Experimental

2.1. Formation and repair of defects in $BiPO_4$

Precursor $BiPO_4$ nanorod was obtained by reflux in 100 °C water for 48 h [4]. 1.0 g $BiPO_4$ and 2.0 mL ethanol were added into agate jar and mixed evenly, and different sizes of agate balls were added subsequently. Afterwards the mixtures were ball-milled at the rate of 300 rpm for different time and at different rate for 2.0 h on the XQM-4.0 planetary ball mill, and then the samples were dried in air to remove ethanol completely to obtain defect $BiPO_4$. At last, the defect $BiPO_4$ formed at 300 rpm for 2.0 h were calcined in the range of 200–600 °C for 4.0 h or refluxed at 100 °C in water for 12.0–48.0 h to repair its defects.

2.2. Evaluation of photocatalytic activity and photoelectrochemical performance

The photocatalytic activity of $BiPO_4$ were evaluated on the degradation of methylene blue (MB) in aqueous solution under 20 W 254 nm UV lamp and the average light intensity was 1.0 mW cm^{-2}. 25 mg photocatalyst was added into 50 mL 3.0×10^{-5} mol L^{-1} MB aqueous solution. The suspension was ultrasonically dispersed for 0.5 h and magnetically stirred for 1.0 h in dark to obtain the establishment of adsorption – desorption equilibrium before UV irradiation. At 20 min intervals, 3.5 mL suspension was taken out and separated through centrifugation (12,000 rpm, 10 min). The concentration of MB solution was analyzed at the maximal absorption band (663 nm) using a Hitachi U-3010 UV–vis spectrophotometer.

The photocurrent and electrochemical impedance spectroscopy (EIS) of $BiPO_4$ were performed on CHI-660B electrochemical system (Shanghai, China) using a standard three-electrode cell with a working electrode (ITO/$BiPO_4$), using a standard calomel electrode (SCE) as reference electrode and a platinum wire as counter electrode. ITO/$BiPO_4$ was prepared by a dip–coating method. Photoelectrochemical properties were measured with an 11 W UV germicidal lamp, and the intensity of light at the film electrode was 1.5 mW cm^{-2} at the wavelength of 254 nm and 0.1 mol L^{-1} Na_2SO_4 electrolyte was used. The photoelectric responses of the photocatalysts with light-on and light-off were measured at 0.0 V. EIS was carried out at the open circuit potential, and a sinusoidal ac perturbation of 5 mV was applied to the electrode over the frequency range of 10^{-2}–10^5 Hz.

2.3. Materials characterization

The crystal-phase structure and crystallinity of $BiPO_4$ samples were characterized by X-ray diffraction (XRD) on a Bruker D8 Advance diffractometer using (Cu Kα = 1.5418 Å, tube voltage = 40 kV, tube current = 20 mA) at a scan rate of 2° min^{-1} in the 2θ range from 10° to 60°.The lattice planes and fringes of $BiPO_4$ were obtained from the high-resolution transmission electron microscope (HRTEM, JEM 2010F), and it was operated at an accelerating voltage of 200 kV. The photoluminescence (PL) emission spectra of $BiPO_4$ samples were measured on HR800 spectrometer with 325 nm exciting light of He-Cd laser under the condition of 77 K. The Raman spectrum of samples were measured at room temperature using HORIBAR 800 microscopic confocal Raman spectrometer in the range of 200–1200 cm^{-1} for three times, and the excitation light was 514.5 nm from an Ar^+ laser with 30 mW output power.

The UV–vis diffuse reflectance absorption spectra of $BiPO_4$ samples were performed on Hitachi U-3010 spectroscope equipped with an integrated sphere attachment in the range of 200–800 nm, and $BaSO_4$ was used as reference. The particle sizes of $BiPO_4$ samples were measured on the HITACHI HT7700 transmission electron microscopy (TEM) with an accelerating voltage 100 kV. The electron paramagnetic resonance (EPR) of photocatalyst was tested on an Endor spectrometer (JEOL ES-ED3X) at 77 K, and the splitting factor g was obtained by taking the signal of manganese (Mn) as standard.

3. Results and discussion

3.1. Controllable formation and repair of defects in $BiPO_4$

The presence and disappearance of defects, as well as the crystal lattice parameters of $BiPO_4$ were examined by HRTEM. As shown in Fig. 1a, the precursor $BiPO_4$was monazite monoclinic structure, with the distances between adjacent lattice fringes measured as 0.307 nm. This corresponds to inter planar distances of $BiPO_4$ (1 2 0) and is in excellent agreement with the literature value of the (1 2 0) lattice distance (JCPDS 80-0209). In addition, the lattice fringes of precursor $BiPO_4$ were very clear. The HRTEM image of ball-milled $BiPO_4$ revealed that its lattice spacing was 0.467 nm, corresponding to the (0 1 1) lattice plane (Fig. 1b). In addition, lattice mismatch, vacancy defects and lots of plane defects were shown in the (0 1 1) lattice plane. At the same time, the partial lattice fringes were very obscure. These phenomena were mainly ascribed to the formation of many defects generated by ball-milling [27]. Part of the structure disorder and vacancy defects still existed in $BiPO_4$ after the repair of calcination (Fig. 1c), which indicated that the defects of ball-milled $BiPO_4$ were not completely repaired via calcination. However, reflux could better repair the defects of $BiPO_4$ than calcination (Fig. 1c and d), and the lattice fringes after reflux were very clear.

The UV–vis diffuse reflectance spectra (DRS) of the precursor $BiPO_4$, $BiPO_4$ ball-milled at 300 rpm for 2.0 h, defect $BiPO_4$ repaired by calcination at 400 °C for 4.0 h in air and $BiPO_4$ repaired by reflux in water solution at 100 °C for 4.0 h are shown in Fig. 2. The absorption band edge of precursor $BiPO_4$ was at about 300 nm. Ball-milling induced a 100 nm red shift in the absorption band edge of $BiPO_4$ and the absorption intensity in the range of 300–500 nm was also obviously enhanced, which was ascribed to the defect induced by ball-milling [23,27,28]. The defect of $BiPO_4$ generated via ball-milling would induce the ascending of valence band maximum and the descending of conduction band minimum to some degree, so the band gap decreased corresponding with $BiPO_4$ with OH defect [29]. The absorption band edges of defect $BiPO_4$ repaired via calcination and reflux shifted to shorter wavelength, but they couldn't return to the position of absorption band edge of precursor $BiPO_4$. The change rule of UV–vis DRS further illustrated that the majority of defects in $BiPO_4$ could be repaired via calcination and reflux.

PL spectrum is an important method to study the defect of photocatalysts [10,27]. $BiPO_4$, as a wide band gap photocatalyst, its valence band is made up of O 2p, Bi 6s, P 3s and P 3p and its conduction band is made up of Bi 6p [30]. Under the excitation of 325 nm wavelength, the characteristic green luminescence at 502 nm and blue luminescence at 441 nm were observed in precursor $BiPO_4$, and the stronger green luminescence was ascribed to the transition of Bi^{3+} from ^3P_J to $^1S_0$ (Fig. 3) [31,32]. The PL intensity of ball-milled $BiPO_4$ is much higher than that of precursor $BiPO_4$ in the range of 400–600 nm, which is caused by many defects generated via ball-milling [9,10,27]. According to literature [27], these defects could be assigned to V_o, O_i, O_O^X and Bi_{Bi}. The more the defects are, the stronger the PL signal is. In general, the strong PL signal means high recombination rate of photo-generated charges and indicate slow photocatalytic performance. Therefore, the ball-milled $BiPO_4$ possessed the lowest photocatalytic activity among the four samples. On the other hand, the PL signals of defect repaired $BiPO_4$ by calcination and reflux became significantly weaker, which indicated

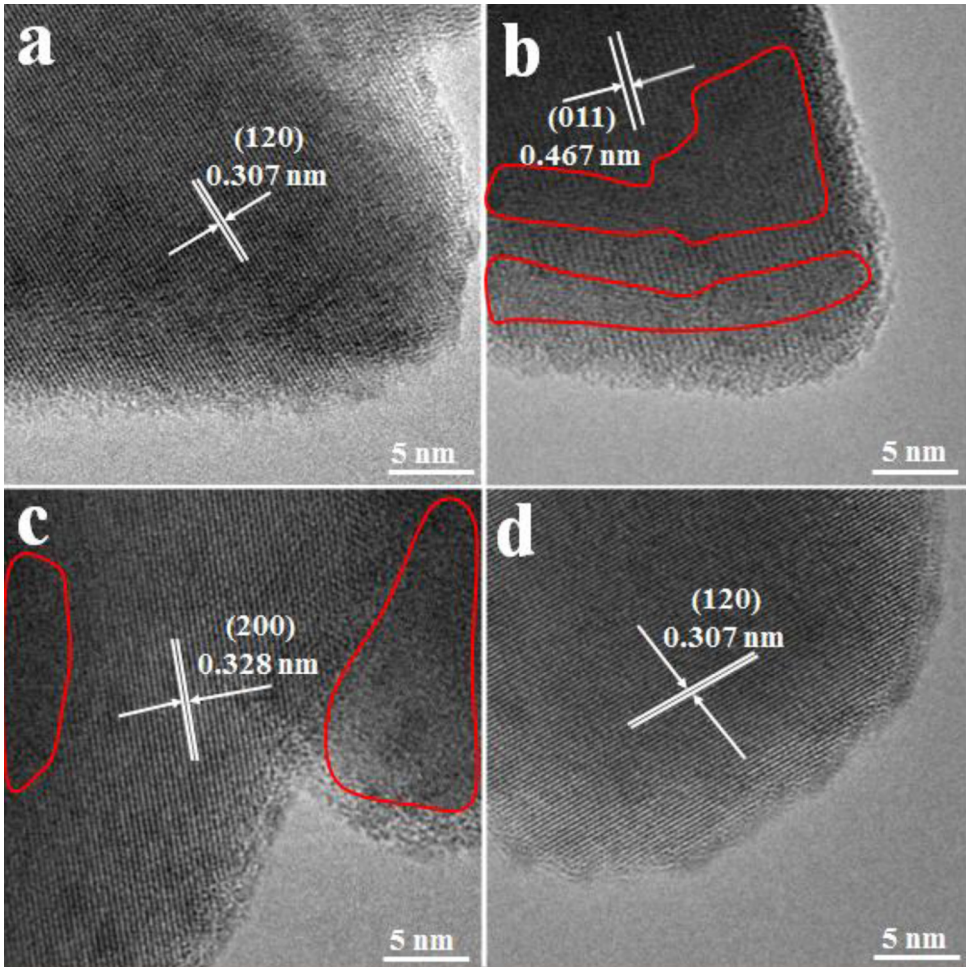

Fig. 1. The HRTEM images of $BiPO_4$ (a), $BiPO_4$ ball-milled at 300 rpm for 2.0 h (b), defect $BiPO_4$ repaired by calcination at 400 °C for 4.0 h in air (c) and defect $BiPO_4$ repaired by reflux at 100 °C for 24.0 h in water solution (d).

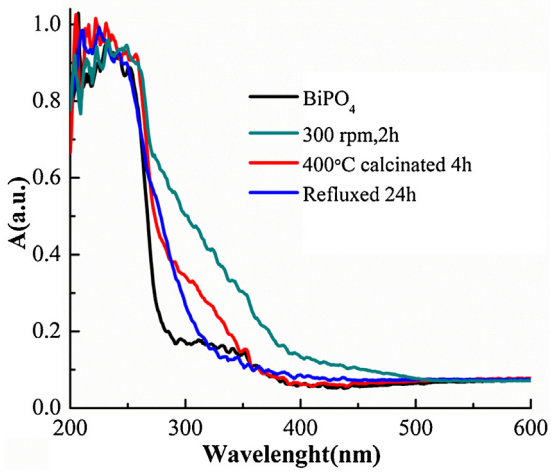

Fig. 2. The UV–vis DRS of precursor $BiPO_4$, $BiPO_4$ ball-milled at 300 rpm for 2.0 h, defect $BiPO_4$ repaired by calcination at 400 °C for 4.0 h and reflux at 100 °C for 24.0 h.

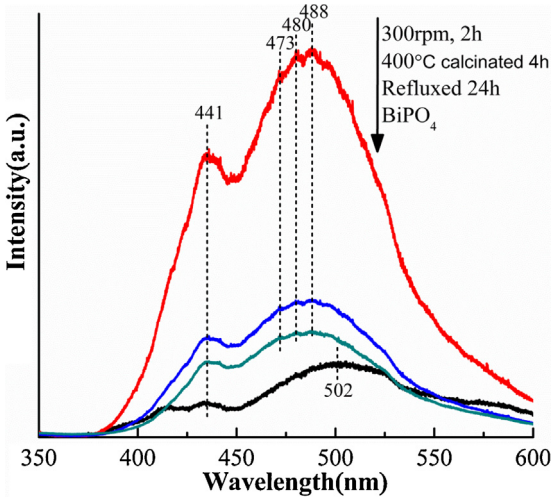

Fig. 3. PL spectra of precursor $BiPO_4$, $BiPO_4$ ball-milled at 300 rpm for 2.0 h, defect $BiPO_4$ repaired by calcination at 400 °C for 4.0 h and reflux at 100 °C for 4.0 h in water solution (excitation wavelength: 325 nm).

that the number of defects in $BiPO_4$ decreased, and thus recovering the quick separation of the photo-generated charges.

In order to further testify the defect structure and characteristics of $BiPO_4$, the EPR was performed at 77 K in liquid N_2 surroundings (Fig. 4). Because the electrons of Bi^{3+}, P^{5+} and O^{2-} in precursor $BiPO_4$ were all paired electrons, no EPR signal was observed. In the crystal structure of $BiPO_4$, one Bi and eight O atoms formed eight ligand structure; one P and four O atoms formed four ligand structure; Bi and P atoms are connected by O and they are in 1:1 proportion [33]. However, a strong EPR signal at about g = 2.001 was observed in ball-milled $BiPO_4$, defect repaired $BiPO_4$ by calcination and defect

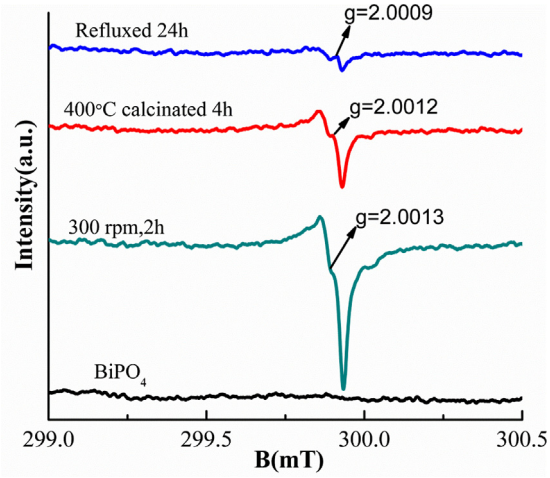

Fig. 4. The EPR spectra of precursor $BiPO_4$, $BiPO_4$ ball-milled at 300 rpm for 2.0 h, defect $BiPO_4$ repaired by calcination at 400 °C for 4.0 h and reflux at 100 °C for 4.0 h.

repaired $BiPO_4$ by reflux, which was attributed to neutral oxygen vacancies (V_o) [2,9,10]. The EPR intensity of ball-milled $BiPO_4$ at g∼2.001 was the highest and that of $BiPO_4$ repaired by calcination and reflux became lower.

The morphology of precursor $BiPO_4$ was nanorod (Fig. 5a) [4], but it would be severely destroyed by ball-milling (Fig. 5b and c). Under the compressive and shear stress of ball-milling, $BiPO_4$ nanorods underwent deformation, which meant that these nanorods became shorter and some of them transformed to a lot of powder particles. The nanorods of ball-milled $BiPO_4$ treated by calcination and reflux were similar to that of ball-milled $BiPO_4$, but their length was shorter than that of precursor $BiPO_4$ (Fig. 5d and f). At the same time, the powder particles of repaired $BiPO_4$similar to the amorphous structure disappeared after calcination and reflux, and a lot of spherical particles were formed around $BiPO_4$ nanorods.

Based on the XRD and Raman results, defect of $BiPO_4$ didn't affect its crystal structure. It can be seen in Figs. S1 and S2 that the crystal structures of ball-milled $BiPO_4$ and repaired $BiPO_4$ after calcination and reflux were the same as that of precursor $BiPO_4$. They were all mainly made up of monazite monoclinic phase and minor of them were hexagonal phase. However, the Raman intensity of ball-milled $BiPO_4$ after 600 cm^{-1} was enhanced on the whole, which could be attributed to the strong fluorescence excited by 325 nm laser irradiation.

3.2. Photocatalytic activity and photocurrents of defect $BiPO_4$

The photocatalytic activity of the precursor $BiPO_4$ and the $BiPO_4$ ball-milled at 300 rpm for different time and at different ball-milling rotating rate for 2.0 h are shown in Fig. 6. The photocatalytic activities of defect $BiPO_4$ were all lower than that of precursor $BiPO_4$, which was caused by the formation of many bulk defects generated from high energy of ball-milling. The results are accorded with the change of photocatalytic performance of TiO_2 and ZnO before and after ball-milling [27,28]. When the rate of ball-milling was 300 rpm, with the ball-milling time prolonging, more bulk defects were generated in $BiPO_4$; at the same time, the photocatalytic activity also decreased gradually (Fig. 6a). When the ball-milling time was 1.0 h and 2.0 h at 300 rpm ball-milling rate, the photocatalytic activity of $BiPO_4$ decreased obviously. The apparent rate constant of $BiPO_4$ ball-milled for 2.0 h on the photocatalytic degradation of MB was 0.0107 min^{-1}, which was about half of that of precursor $BiPO_4$ ($k = 0.0229\ min^{-1}$). When the ball-milling time were prolonged to 2.0–5.0 h, the photocatalytic activity of $BiPO_4$ decreased very slowly, which illustrated that the bulk defects generated more and more weakly with the ball-milling time further prolonging. The apparent rate constant of $BiPO_4$ ball-milled for 5.0 h was 0.069 min^{-1}, which was about 1/3 of precursor $BiPO_4$. When the ball-milling time was 2.0 h, with the ball-milling rate increasing,

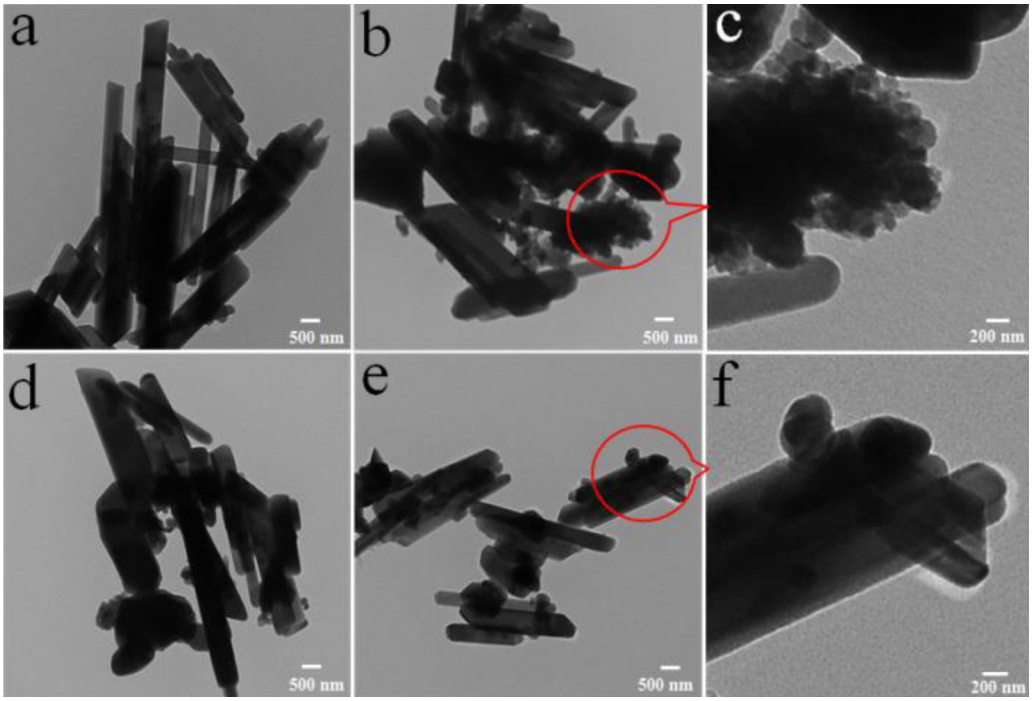

Fig. 5. TEM images of $BiPO_4$ (a), $BiPO_4$ ball-milled at 300 rpm for 2.0 h (b and c), defect $BiPO_4$ repaired by calcination at 400 °C for 4.0 h in air (d) and $BiPO_4$ repaired by reflux at 100 °C for 4.0 h in water (e and f).

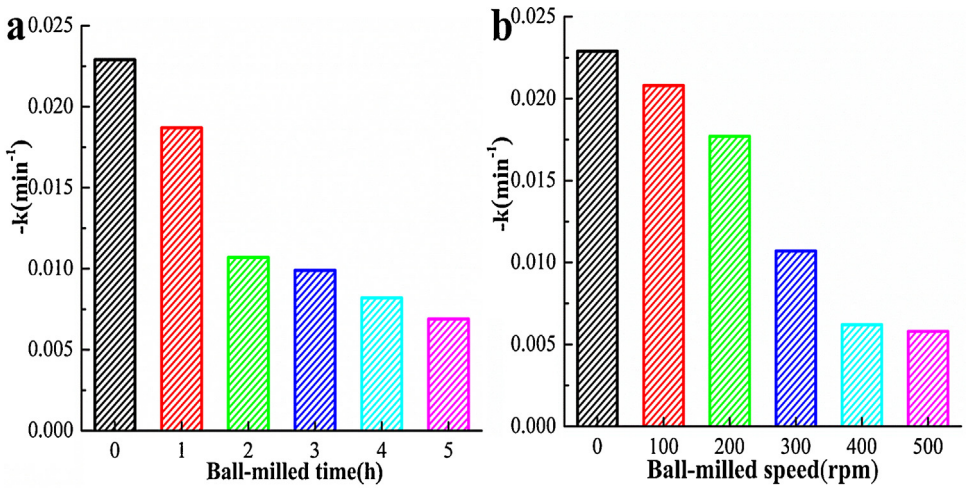

Fig. 6. The apparent rate constants of photocatalytic oxidation degradation of MB over $BiPO_4$ ball-milled at 300 rpm for different time (a) and at different ball-milling rotating rate for 2.0 h (b).

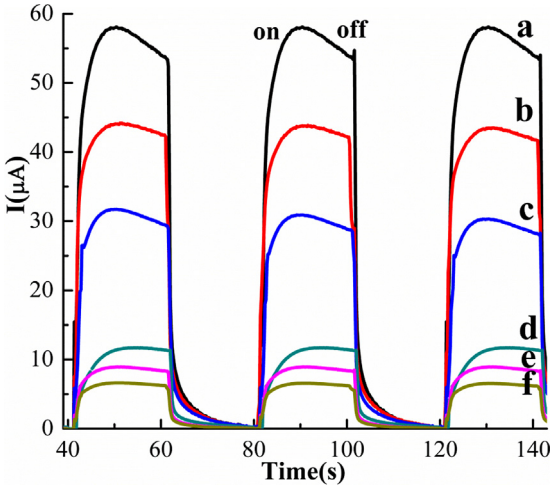

Fig. 7. The photocurrents of precursor $BiPO_4$ and $BiPO_4$ ball-milled on different conditions under 254 nm UV light irradiation (a) precursor $BiPO_4$; (b) $BiPO_4$ ball-milled at 100 rpm for 2.0 h; (c) $BiPO_4$ ball-milled at 300 rpm for 1.0 h; (d) $BiPO_4$ ball-milled at 300 rpm for 2.0 h; (e) $BiPO_4$ ball-milled at 300 rpm for 5.0 h; (f) $BiPO_4$ ball-milled at 500 rpm for 2.0 h).

the photocatalytic activity of $BiPO_4$ gradually decreased (Fig. 6b). The increase of ball-milling rate would transmit more mechanical energy to $BiPO_4$, so more bulk defects would be generated and then the photocatalytic activity of $BiPO_4$ decreased.

During the process of photocatalytic reaction, the separation and transfer of photo-generated electrons and holes for photocatalysis are the key steps that determine photocatalytic efficiency. The photocurrent of photocatalyst under light irradiation could illustrate the separation and transfer of photo-generated charges [34]. The photocurrents of precursor $BiPO_4$ and ball-milled $BiPO_4$ on different conditions are shown in Fig. 7. The photocurrents were stable and reversible at light-on and light-off for all $BiPO_4$ samples under 254 nm UV light irradiation. The photocurrent of precursor $BiPO_4$ was the highest (about 55 μA), and that of the ball-milled ones were all weaker than it. When the ball-milling rate was 300 rpm, with increasing ball-milling time, the photocurrents of $BiPO_4$ would decrease gradually, which indicated that the bulk defect would become the recombination center of photo-generated charges and inhibit its quick separation and transfer. Meanwhile, with the increase of ball-milling rate, more bulk defects would form, leading to the gradual decrease of the photocurrents of $BiPO_4$.

3.3. *Photocatalytic activity and photocurrents of defect repaired $BiPO_4$*

Calcination and reflux were used to repair the defect of $BiPO_4$ generated by ball-milling at 300 rpm for 2.0 h. The photocatalytic activities of the defect and defect repaired $BiPO_4$ are shown in Fig. 8. As it is known, calcination could make material recrystallize and eliminate part of defect structure. The photocatalytic activity of TiO_2, Ga_2O_3 and CdS calcined at appropriate temperatures would be enhanced obviously [35–37]. Moreover, reflux could also change the morphology and structure of materials and eliminate defects. For instance, the photocatalytic activity of C_3N_4 refluxed in methanol and sulphuric acid solution were greatly enhanced [38,39]. The photocatalytic performance of defect $BiPO_4$ repaired via calcination in the range of 200–600 °C were all higher than that of defect $BiPO_4$, but lower than that of precursor $BiPO_4$ (Fig. 8a). In the range of 200–400 °C, with increasing the calcination temperature, the photocatalytic activity of defect $BiPO_4$ repaired were enhanced gradually. Further increasing the calcination temperature above 400 °C, the photocatalytic activity of the defect repaired $BiPO_4$ decreased gradually. Therefore, proper calcination temperature could improve the photocatalytic performance of $BiPO_4$, but too high calcination temperature would change the crystal structure of $BiPO_4$ or induce agglomeration and further decrease the photocatalytic performance [35,36]. Hence, the best calcination temperature for defect $BiPO_4$ was 400 °C, and the apparent rate constant of defect $BiPO_4$ repaired at 400 °C on the photocatalytic degradation of MB was 0.0162 min^{-1}, which was about 1.5 and 0.71 times as high as that of defect $BiPO_4$ ball-milled at 300 rpm for 2.0 h and precursor $BiPO_4$. The photocatalytic activity of defect $BiPO_4$ repaired via reflux in water was enhanced obviously, and the apparent rate constant for the photocatalytic degradation of MB over $BiPO_4$ refluxed for 24.0 h was 0.0209 min^{-1}, which was about 1.95 times than that of defect $BiPO_4$ but lower than that of precursor $BiPO_4$. Both calcination and reflux could repair the defect in $BiPO_4$ and thus improve the photocatalytic performance, but reflux could have better repair effect for defect $BiPO_4$ than calcination.

The photocurrents of defect $BiPO_4$ ball-milled at 300 rpm for 2.0 h, defect $BiPO_4$ repaired via calcination and reflux under 254 nm UV light irradiation are shown in Fig. S3. The photocurrents of defect

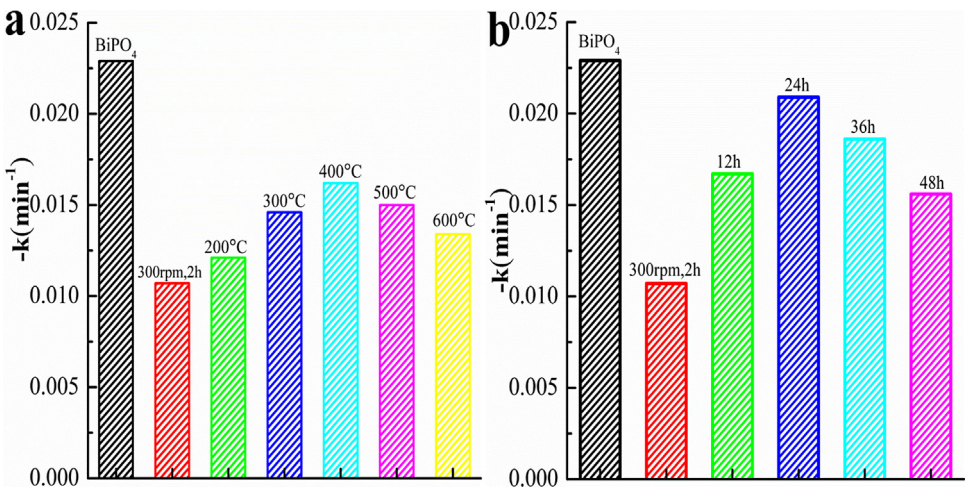

Fig. 8. The apparent rate constants of photocatalytic oxidation degradation of MB over defect $BiPO_4$ repaired via calcination at different temperatures for 4.0 h (a) and reflux in water for different time (b).

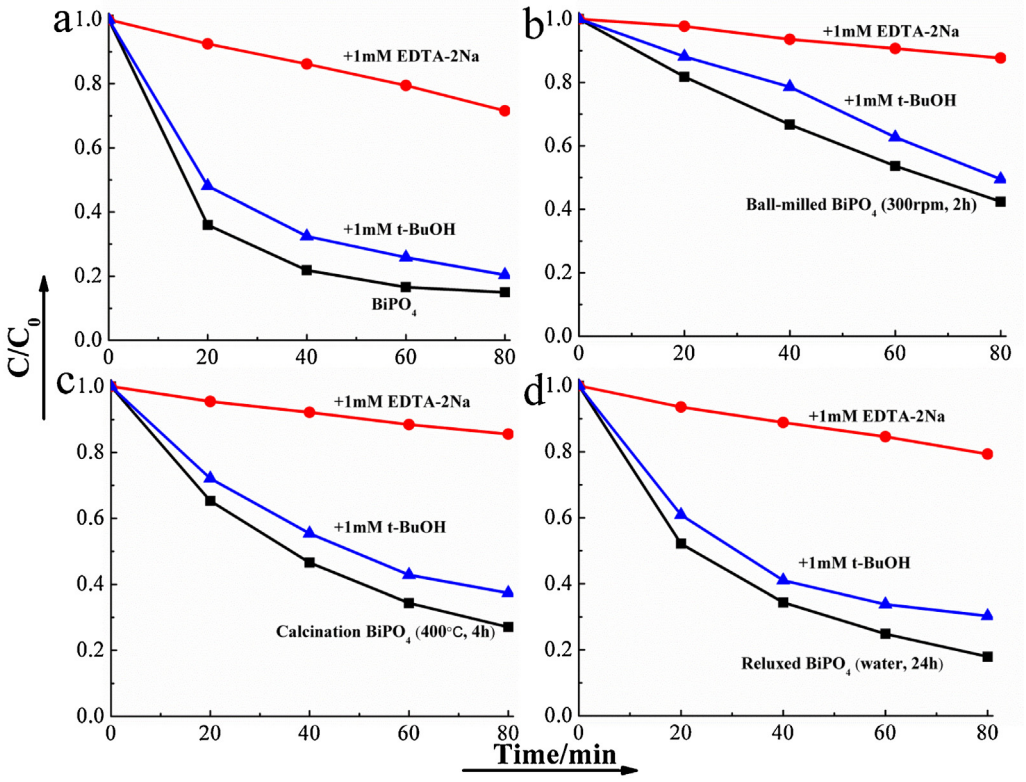

Fig. 9. The plots of photo-generated charges trapping on the photocatalytic degradation of MB over precursor $BiPO_4$ (a), defect $BiPO_4$ ball-milled at 300 rpm for 2 h (b), defect $BiPO_4$ repaired via calcination at 400 °C for 4.0 h (c), defect $BiPO_4$ repaired via reflux at 100 °C for 24.0 h (d).

$BiPO_4$ repaired by calcination and reflux were all higher than that of defect $BiPO_4$. The above results further testified that calcination and reflux could repair and decrease vast bulk defect of ball-milled $BiPO_4$, which promoted the quick separation of photo-generated charges and enhanced the photocatalytic performance of $BiPO_4$.

3.4. Mechanism of defect on the photocatalytic performance of $BiPO_4$

The photocatalytic mechanism of semiconductor photocatalyst could be verified by trapping experiment of radicals and holes, usually using ethylenediamine tetraacetic acid disodium salt (EDTA-2Na) and tertiary butyl alcohol (*t*-BuOH) as hole and hydroxyl radical scavengers [27,30]. The oxidation species in the photocatalytic degradation of MB by precursor $BiPO_4$, defect $BiPO_4$ ball-milled at 300 rpm for 2.0 h, defect $BiPO_4$ repaired via calcination at 400 °C for 4.0 h and defect $BiPO_4$ repaired via reflux at 100 °C for 24.0 h are shown in Fig. 9. In the $BiPO_4$ system, the photocatalytic performance decreased greatly by addition of EDTA-2Na but changed very slightly by addition of *t*-BuOH (Fig. 9a), suggesting that the photo-generated holes are the main oxidative species of $BiPO_4$ and the hydroxyl radicals only played an assistant role [9,10].

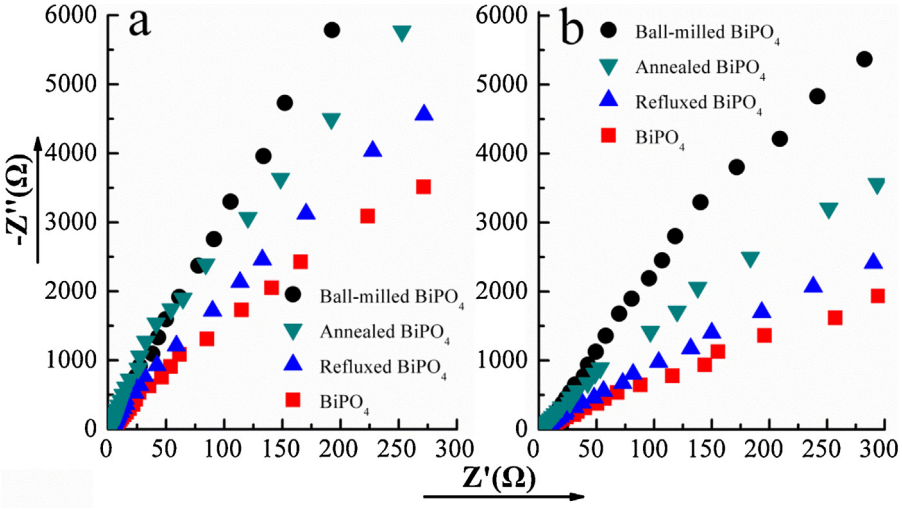

Fig. 10. The EIS Nyquist plots of $BiPO_4$ thin film electrodes in dark (a) and under UV light irradiation (b).

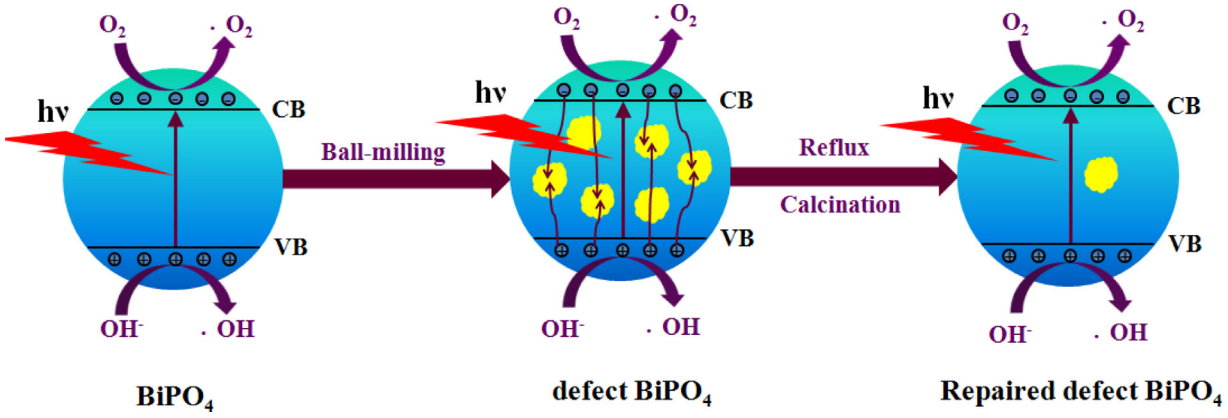

Scheme 1. The mechanism of charge separation and photocatalytic process over $BiPO_4$ under UV light irradiation.

Moreover, the main oxidative species of defect $BiPO_4$ ball-milled at 300 rpm for 2.0 h (Fig. 9b), defect repaired $BiPO_4$ via calcination at 400 °C for 4.0 h (Fig. 9c) and via reflux at 100 °C for 24.0 h (Fig. 9d) were all photo-generated holes, which proved that defect couldn't change the active oxidative species of $BiPO_4$ [22].

As is well known, the separation efficiency of photo-generated charges is a key factor to influence the photocatalytic activity. The efficiency of photo-generated electron-hole pairs can be evaluated by the typical electrochemical impedance spectra (EIS). The arc radius on the EIS spectra reflects the solid state interface layered resistance and the surface charges transfer resistance. The smallest arc radius on the EIS Nyquist plot indicates an efficient separation of the photo-generated electron-hole, and vice versa [39]. The EIS plots of precursor $BiPO_4$, defect $BiPO_4$ ball-milled at 300 rpm for 2.0 h, the defect $BiPO_4$ repaired via calcination at 400 °C for 4.0 h and via reflux at 100 °C for 24.0 h are shown in Fig. 10. The Nyquist arc radii of precursor $BiPO_4$ in dark and under UV light irradiation were the smallest among the four $BiPO_4$ samples, suggesting that the reaction rate on this electrode surface was the maximum and the electrode resistance was the smallest, so the separation of photo-generated electrons and holes in precursor $BiPO_4$ was the fastest. However, the Nyquist arc radii of the defect $BiPO_4$ ball-milled was the biggest, so the reaction rate on this electrode surface was the smallest and the electrode resistance was the maximum; at the same time, the separation efficiency of photo-generated electron-hole pairs in this sample was very low. The Nyquist arc radii of defect $BiPO_4$ repaired via calcination and reflux both in dark and under UV light irradiation were between that of precursor $BiPO_4$ and defect $BiPO_4$.

From the above results, a probable mechanism of charge separation and photocatalytic process over $BiPO_4$ under UV light irradiation is inferred in Scheme 1. Under the UV light irradiation, the electrons of $BiPO_4$ were transited into conduction band and holes remained in the valance band, and then they reacted with O_2 and OH^- respectively to form $\cdot O_2$ and $\cdot OH$ to degrade organic pollutants. The bulk defect of $BiPO_4$ formed by ball-milling became the recombination center of photo-generated charges and restrained its efficient separation. The defect $BiPO_4$ repaired via calcination and reflux revised many bulk defects and enhanced the separation efficiency of photo-generated electron-hole pairs, which further improved the photocatalytic activity of $BiPO_4$.

4. Conclusions

The defects in $BiPO_4$ were controllably formed by ball-milling, and most of them were repaired via calcination and reflux. The influence of defects on the photocatalytic and photoelectric performance of $BiPO_4$ have been elucidated. This work shed deeper light on the effect rule of bulk defect on photocatalytic performance of $BiPO_4$, and provided a referenced method for repairing the defect

of other semiconductor photocatalysts and further improving their photocatalytic activity.

Acknowledgements

This work was partly supported by National Basic Research Program of China (2013CB632403), National High Technology Research and Development Program of China (2012AA062701) and Chinese National Science Foundation (21437003 and 21373121).

Appendix A. Supplementary data

Supplementary data associated with this article can be found, in the online version, at http://dx.doi.org/10.1016/j.apcatb.2016.01.012.

References

[1] C. Pan, Y. Zhu, Catal. Sci. Technol. 5 (2015) 3071–3083.
[2] Z. Wei, Y. Liu, J. Wang, R. Zong, W. Yao, J. Wang, Y. Zhu, Nanoscale 7 (2015) 13943–13950.
[3] C. Pan, Y. Zhu, Environ. Sci. Technol. 44 (2010) 5570–5574.
[4] Y. Zhu, Y. Liu, Q. Ling, Y. Lv, H. Wang, Y. Zhu, Acta Phys.—Chim. Sin. 29 (2013) 576–584.
[5] Y. Liu, Y. Lv, Y. Zhu, D. Liu, R. Zong, Y. Zhu, Appl. Catal. B: Environ. 147 (2014) 851–857.
[6] Y. Liu, W. Yao, D. Liu, R. Zong, M. Zhang, X. Ma, Y. Zhu, Appl. Catal. B: Environ. 163 (2015) 547–553.
[7] C. Pan, J. Xu, Y. Wang, D. Li, Y. Zhu, Adv. Funct. Mater. 22 (2012) 1518–1524.
[8] S. Wu, H. Zhengn, Y. Wu, W. Lin, T. Xu, M. Guan, Ceram. Int. 40 (2014) 14613–14620.
[9] Y. Lv, Y. Liu, Y. Zhu, Y. Zhu, J. Mater. Chem. A 2 (2014) 1174–1182.
[10] Y. Lv, Y. Zhu, Y. Zhu, J. Phys. Chem. C 117 (2013) 18520–18528.
[11] Q. Zhang, H. Tian, N. Li, M. Chen, F. Teng, CrystEngComm 16 (2015) 8334–8339.
[12] M. Kong, Y. Li, X. Chen, T. Tian, P. Fang, F. Zheng, X. Zhao, J. Am. Chem. Soc. 133 (2011) 16414–16417.
[13] S.G. Kumar, K.S.R.K. Rao, RSC Adv. 5 (2015) 3306–3351.
[14] J. Yan, G. Wu, N. Guan, L. Li, Z. Li, X. Cao, Phys. Chem. Chem. Phys. 15 (2013) 10978–10988.
[15] M.J. Llansola-Portoles, J.J. Bergkamp, D. Finkelstein-Shapiro, B.D. Sherman, G. Kodis, N.M. Dimitrijevic, D. Gust, T.A. Moore, A.L. Moore, J. Phys. Chem. A 118 (2014) 10631–10638.
[16] T.L. Thompson, J.T. Yates, Top. Catal. 35 (2005) 197–210.
[17] X. Pan, M. Yang, X. Fu, N. Zhang, Y. Xu, Nanoscale 5 (2013) 3601–3614.
[18] S. Ali Ansari, M. Mansoob Khan, M. Omaish Ansari, M. Hwan Cho, Sol. Energy Mater. Sol. Cells 141 (2015) 162–170.
[19] B. Henkel, T. Neubert, S. Zabel, C. Lamprecht, C. Selhuber-Unkel, K. Rätzke, T. Strunskus, M. Vergöhl, F. Faupel, Appl. Catal. B: Environ. 180 (2016) 362–371.
[20] Z. Pei, S. Weng, P. Liu, Appl. Catal. B: Environ. 180 (2016) 463–470.
[21] F. Kayaci, S. Vempati, C. Ozgit-Akgun, I. Donmez, N. Biyikli, T. Uyar, Appl. Catal. B: Environ. 176–177 (2015) 646–653.
[22] Z. Pei, L. Ding, J. Hu, S. Weng, Z. Zheng, M. Huang, P. Liu, Appl. Catal. B: Environ. 142–143 (2013) 736–743.
[23] J. Wang, W. Jiang, D. Liu, Z. Wei, Y. Zhu, Appl. Catal. B: Environ. 176–177 (2015) 306–314.
[24] Y. Huang, B. Long, M. Tang, Z. Rui, M.-S. Balogun, Y. Tong, H. Ji, Appl. Catal. B: Environ. 181 (2016) 779–787.
[25] J. Shi, H. Cui, Z. Liang, X. Lu, Y. Tong, C. Sua, H. Liu, Energy Environ. Sci. 4 (2011) 466–470.
[26] T. Jing, Y. Dai, W. Wei, X. Ma, B. Huang, Phys. Chem. Chem. Phys. 16 (2014) 18596–18604.
[27] D. Chen, Z. Wang, T. Ren, H. Ding, W. Yao, R. Zong, Y. Zhu, J. Phys. Chem. C 118 (2014) 15300–15307.
[28] J.O. Carneiro, S. Azevedo, F. Fernandes, E. Freitas, M. Pereira, C.J. Tavares, S. Lanceros-Mendez, V. Teixeira, J. Mater. Sci. 49 (2014) 7476–7488.
[29] C. Pan, J. Xu, Y. Chen, Y. Zhu, Appl. Catal. B: Environ. 115–116 (2012) 314–319.
[30] Y. Hizhnyi, S. Nedilko, V. Chornii, K. Terebilenko, V. Boykob, Phys. Status Solidi 8 (2012) 46–47.
[31] F. Xue, H. Li, Y. Zhu, S. Xiong, X. Zhang, T. Wang, X. Liang, Y. Qian, J. Solid State Chem. 182 (2009) 1396–1400.
[32] M. Guan, J. Sun, F. Tao, Z. Xu, Cryst. Growth Des. 8 (2008) 2694–2697.
[33] C. Pan, D. Li, X. Ma, Y. Chen, Y. Zhu, Catal. Sci. Technol. 1 (2011) 1399–1405.
[34] T. Xu, H. Zheng, P. Zhang, W. Lin, Y. Sekiguchi, J. Mater. Chem. A 3 (2015) 19115–19122.
[35] Q. Chen, H. Liu, Y. Xin, X. Cheng, Electrochim. Acta 111 (2013) 284–291.
[36] X. Wang, Q. Xu, M. Li, S. Shen, X. Wang, Y. Wang, Z. Feng, J. Shi, H. Han, C. Li, Angew. Chem. Int. Ed. 51 (2012) 13089–13092.
[37] G. Chen, D. Li, F. Li, Y. Fan, H. Zhao, Y. Luo, R. Yu, Q. Meng, Appl. Catal. A: Gen. 443–444 (2012) 138–144.
[38] X. Bai, L. Wang, R. Zong, Y. Zhu, J. Phys. Chem. C 117 (2013) 9952–9961.
[39] J. Xu, L. Zhang, R. Shi, Y. Zhu, J. Mater. Chem. A 1 (2013) 14766–14772.